High-performance thermal emitters based on laser engineered metal surfaces

Zolotovskaya, Svetlana A.; Wackerow, Stefan; Neupert, Holger; Barnes, Michael J.; Cid, Lorena V.; Teissandier, Benoit

Published in:
Optical Materials Express

DOI:
10.1364/OME.381668

Publication date:
2020

Document Version
Publisher's PDF, also known as Version of record

Research Article | Vol. 10, No. 2 / 1 February 2020 / Optical Materials Express 622

Optical Materials EXPRESS

High-performance thermal emitters based on laser-engineered metal surfaces

SVETLANA A. ZOLOTOVSKAYA,[1,*] STEFAN WACKEROW,[1] HOLGER NEUPERT,[2] MICHAEL J. BARNES,[2] LORENA VEGA CID,[2] BENOIT TEISSANDIER,[2] ANA TERESA PEREZ FONTENLA,[2] AND AMIN ABDOLVAND[1]

[1]*Materials Science & Engineering Research Cluster, School of Science and Engineering, University of Dundee, Dundee DD1 4HN, United Kingdom*
[2]*CERN – European Organization for Nuclear Research, CH-1211 Geneva 23, Switzerland*
[*]*sazolotovskaya@dundee.ac.uk*

Abstract: Effective thermal management is of paramount importance for all high-temperature systems operating under vacuum. Cooling of such systems relies mainly on radiative heat transfer requiring high spectral emissivity of surfaces, which is strongly affected by the surface condition. Pulsed laser structuring of stainless steel in air resulted in the spectral hemispherical emissivity values exceeding 0.95 in the 2.5–15 μm spectral region. The effects of surface oxidation and topography on spectral emissivity as well as high temperature stability of the surface structures were examined. High performance stability of the laser textured surfaces was confirmed after thermal aging studies at 320°C for 96 hours.

1. Introduction

The development of new thermal management solutions is essential to enable future high energy, space and communication systems. Radiative heat transfer is the fastest energy transfer mechanism and becomes critically important in high-temperature systems due to the fourth-power temperature dependence of radiated heat energy according to the Stefan-Boltzmann law. Unlike conduction and convection, radiative energy transfer does not require the presence of an intervening medium, thus it suffers no attenuation in vacuum. For opaque materials such as metals, radiation is considered to be a surface phenomenon which exhibits wavelength and temperature dependent behavior. Emissivity is then a measure of how closely the surface approximates a blackbody, for which emissivity is unity ($\varepsilon = 1$). Absorption (α) and reflection (R) determine radiative properties of opaque surfaces, and are related to emissivity in thermal equilibrium state via Kirchhoff's law:

$$\varepsilon\,(\lambda,\ \theta, T) = \alpha(\lambda,\ \theta, T) = 1 - R(\lambda,\ \theta, T) \tag{1}$$

where $\lambda,\ \theta, T$ indicate spectral, directional and temperature dependencies.

This fundamental relationship is the basis for the recently emerged topographical approaches to emissivity control [1] as well as for more traditional surface treatment techniques, such as oxidation and surface roughening [2]. Narrowband thermal emission control is achieved via periodic nano- and micropatterning which allows for the utility of photonic resonances for enhancement and suppression of thermal radiation in particular spectral regions. These selective thermal emitters [3–9] are desired for energy harvesting applications, such as in the field of solar thermophotovoltaics [10], and for gas sensing applications [11], requiring narrowband light sources. However, for effective radiative cooling, the broadband emissivity control is preferred. Passive radiative cooling solutions have been intensively investigated for space [12] and high energy applications [13,14] where severe mass and power consumption constraints as well as high operating temperatures are imposed. Textured metallic [12] and ceramic [15–17]

#381668 https://doi.org/10.1364/OME.381668
Journal © 2020 Received 28 Oct 2019; revised 16 Dec 2019; accepted 16 Dec 2019; published 29 Jan 2020

Optical Materials EXPRESS

coatings have been shown as good material candidates exhibiting high emissivity ($\varepsilon \geq 0.8$), good temperature and corrosion resistance. However, adhesion, stress resistance and vacuum compatibility of coatings remain a significant concern for applications in high-energy physics and particle accelerators such as the Large Hadron Collider (LHC) at CERN [18–20].

Laser-assisted surface structuring approach has shown great potential for production of high-performance metal thermal emitters [21–24], addressing some intrinsic shortcoming of other fabrication techniques such as materials selection, area limitation and cost. A large variety of surface topographies can be accessed by varying laser treatment parameters (i.e. laser fluence and number of pulses per spot) and processing atmosphere (inert or reactive). Recent demonstrations have been dominated by application of femtosecond (fs) laser sources to direct nano- and microstructuring. High-emissivity performance ($\varepsilon > 0.9$) at 100°C in the spectral range from 4 to 16 μm was attained with a hierarchical surface structure [22], consisting of randomly positioned microcavities with sub-micrometer surface protrusions. High-temperature performance and structural stability up to 1000°C with a moderate emissivity performance ($0.4 < \varepsilon < 0.5$) in the spectral range from 2 to 15 μm was shown for the microhole array arrangements [23]. An earlier report focused on the implementation of nanosecond pulse laser structuring [24] showed some evidence that high-emissivity performance at elevated temperatures (700 - 1100°C) can be achieved with the microcolumn array structures.

Here, nanosecond (ns) pulsed laser surface structuring of stainless-steel was investigated in order to establish optimal surface topography with high spectral emissivity in the region from 2.5 to 25 μm. The effects of surface oxidation and topography on spectral emissivity as well as high temperature stability of the surface structure were also examined.

2. Experimental methods

For this study, AISI 304L stainless steel foils (with the nominal composition in wt.%: (Balance) Fe, (18) Cr, (10) Ni, (2) Mn, (1) Si, (0.045) P, (0.03) C, (0.015) S, (0.1) N) were used for the laser treatment. The 1-mm thick steel sheets were cut in 20×20 mm squares and were used as received with no further surface preparation except cleaning and degreasing. The surface roughness of untreated samples was measured to be $R_a = 0.043$ and 0.082 μm for the surface profiles taken at 90° to each other using DektakXT stylus profiler (Bruker) equipped with a 2-μm stylus.

A self-assembled microstructuring with ns laser pulses, previously demonstrated in Refs. [24–26], was chosen as the most promising approach for the formation of a regular surface topography capable of withstanding the bake out process conducted in air at 320°C. A 1064-nm Nd:YVO_4 laser with a maximum average power of 20 W and a pulse length of 8 ns operating at 20 kHz was utilized for the laser treatment in *air* and under *nitrogen*. The laser beam with a Gaussian intensity profile ($M^2 \sim 1.1$) was focused onto the steel surface using a flat-field scanning lens system. The laser beam spot size at the focal plane was measured to be 70 μm at the $1/e^2$ intensity level. The energy fluences in the range from ~3.6 to 18.5 J/cm^2 were employed for the surface structuring. The laser beam was raster scanned over the surface at different speeds from 10 to 23 mm/s in a crossline manner using a computer-controlled two-axis scan head system. The distances between the adjacent scan lines (hatch distance) were adjusted from 50 to 107 μm with the increase in the incident laser fluence. The total number of pulses per spot delivered to the surface was varied from 140 to 1400 for one and ten passes, respectively.

A VERTEX 70 FT-IR spectrometer (Bruker) equipped with a 75-mm diameter gold-coated integrating sphere A562-G was used to determine the spectral hemispherical emissivity of the laser-treated surfaces in the spectral region from 2.5 to 25 μm. Spectra were recorded in direct mode at ~ 5 nm resolution. A beam-steering mirror in the sphere directed the incoming light from the FTIR spectrometer to either the sample port or reference point on the front wall of the sphere (see Fig. 6, Appendix A). With the mirror pointing towards the sample, the angle of incidence was 14.8°, fulfilling typical requirement of near normal light incidence for emissivity

Optical Materials EXPRESS

analysis to reduce polarization effects. The measurement spot size was ~ 4 mm in diameter. A specular exclusion port allows measurements of the diffuse-only or the total (hemispherical) reflectance spectra, which is the sum of diffuse and specular components. In this work, the spectral hemispherical reflectance was determined as a ratio of total reflectance spectra of the sample to the reference point. The spectral hemispherical emissivity was then determined using Kirchhoff's law (Eq. 1). All measurements were taken at room temperature. For each spectrum, 128 scans were averaged with the sample kept in the sample port for the sample and reference spectra to maintain a constant sphere albedo. The number of scans was further increased to 3096 for the best performing surface topography to improve signal-to-noise ratio. The measurements were taken under different sample orientations, for in-plane sample rotation, to establish the influence of the microstructure orientation on the emissivity response.

Chromium-nickel stainless steel acid pickling [27] of the laser processed sample was used in order to isolate individual contributions of oxidation during laser surface structuring in *air*. A mixture of 12% nitric (HNO_3) and 4% hydrofluoric (HF) acids, both by volume, in water was used for pickling at room temperature. HNO_3 is oxidizing in character, whereas HF is reducing. Therefore, in the mixture the oxide-removing feature and the base metal passivating action were combined, hence allowing for gentle removal of the oxide layer without significantly affecting the surface microstructure.

Controlled oxidation of the steel substrates processed in *nitrogen* was performed in air using Carbolite RWF1100 oven. The oxidation temperature was determined based on the temperature used during specific bake out operations in LHC. The lower oxidation boundary was attained after 7 h at 320°C. For the upper limit the temperature was increased to 600°C for 6-h oxidation treatment to speed up the process.

JEOL JSM-7400F scanning electron microscope (SEM) was used to obtain high magnification images of the steel surfaces.

3. Results and discussion

Figure 1(a) shows the spectral hemispherical emissivity responses of the untreated steel and the best performing laser-engineered surface, measured at 22°C, with corresponding surface topographies, see the SEM images in Figs. 1(b) and 1(c). The spectral emissivity performance of the as-received 304L steel substrate demonstrates a monotonic emissivity decay from ~0.3 at 2.5 µm to below 0.1 at longer wavelengths, Fig. 1(a) – *dashed curve*. This characteristically low emissivity behavior of untreated metal surfaces [2] represents a significant practical challenge, limiting the efficiency of temperature management systems. Markedly different behavior of the spectral emissivity was observed after the ns-laser structuring in air, Fig. 1(a) – *solid curve*. Dramatic emissivity increase to ~ 0.97 with almost flat response over a wide spectral range from 2.5 to 14 µm was attained after the laser structuring with a pulse fluence of ~ 3.6 J/cm^2 at a laser beam scanning speed of 10 mm/s, and a 75-µm hatch distance with a total number of pulses per spot equal to 1400. This resulted in the formation of highly organized conical structures with the deepest microcavity formed at the line crossing, see Fig. 1(c). The observed spectral emissivity increase is a result of combined action of the surface oxide layer, promoted by the laser processing in air, and the surface microstructure, formed as a result of the hydrodynamic instabilities of the melt produced on the surface during laser treatment [25,26].

To isolate individual contributions of the surface oxidation and microtopography effects, a set of laser-structured surfaces was produced in a *nitrogen* processing atmosphere, utilizing the laser structuring parameters resulted in the best performing surface topography. Nitrogen (N_2) is a known shielding gas that helps to exclude oxygen from the processing zone, preventing metal oxidation. Although it is reactive at elevated temperatures, it forms only small amount of lattice nitrides at low gas pressures [28,29]. The spectral response of the steel surfaces structured in *nitrogen* show noticeable reduction in the emissivity compared to the *in-air* treated surface, as

Optical Materials EXPRESS

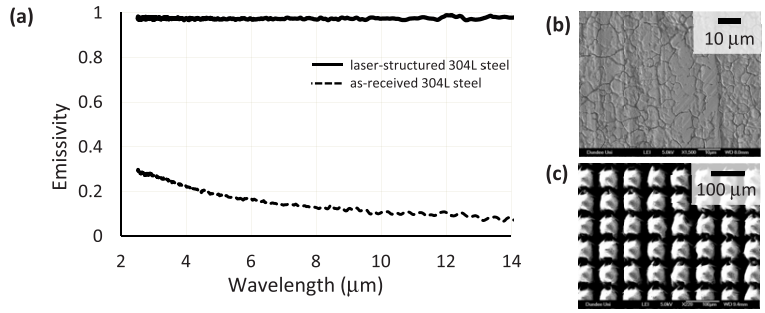

Fig. 1. (a) Spectral hemispherical emissivity responses of the as-received (*dashed curve*) and laser-structured (*solid curve*) 304L steel measured at 22°C. (b) Surface topography of the untreated steel. (c) Surface topography of the steel surface after laser structuring in *air*.

seen from Fig. 2(a). This change in the spectral emissivity behavior can be attributed largely to the microtopography change resulted from the processing in an oxygen-deficient atmosphere, Fig. 2(b). Formation of the highly regular conical structures produced in an *air* environment (Fig. 1(b)) can no longer be supported in the N_2 atmosphere, which promotes formation of a regular structure with a truncated cone microgeometry. This is due to differences in temperature within the processing zone as well as changes in properties of the molten pool. The latter is consistent with some earlier studies where it was shown that the presence of even small amounts of oxygen significantly reduces the surface tension of the liquid metal pool [30]. A similar drop in the spectral emissivity values was observed after the chemical removal of the oxide layer from the *in-air* processed sample which resulted in a comparable truncated cone microstructure, Fig. 2(c).

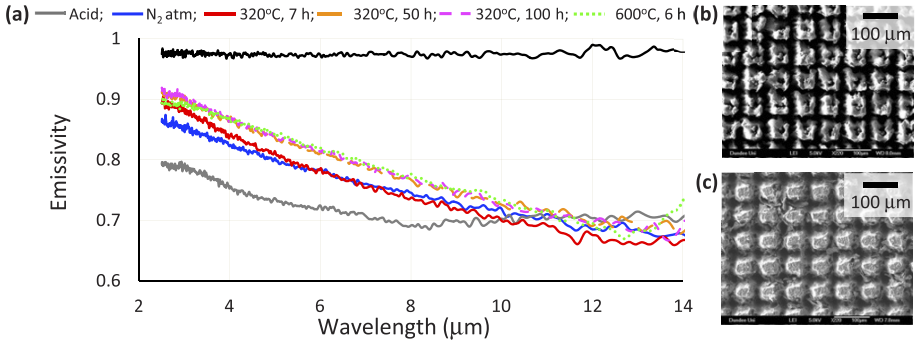

Fig. 2. (a) Spectral hemispherical emissivity responses of the chemically etched and air-oxidized 304L steel surfaces measured at 22°C (emissivity response of the best performing topography shown in black). (b) Surface topography of the steel after laser structuring in *nitrogen* (N_2). (c) Surface topography of the *in-air* laser-structured steel after acid pickling.

Controlled oxidation of the structures produced in the N_2 atmosphere was used to quantify the effect of surface oxidation on the emissivity response. The surface topographies before and after controlled oxidation show no visible change of the microstructure (Appendix A, Fig. 7). The differences in the spectral hemispherical emissivity between the reference (Fig. 2(a), N_2 *atm*) and the oxidized structures are relatively small occurring in the spectral region up to 10 μm for a heavily oxidized structure at 600°C for 6 h. It should be noted that after a 50-h oxidation treatment the oxidation-dependent emissivity increase is no longer observed. This is consistent with a previous work on the emissivity of type 304 and 316 stainless steel [31], and is attributed to a limited oxide layer growth for austenitic alloys with high chromium (Cr) content.

Optical Materials EXPRESS

The effect of microstructure on the hemispherical emissivity was studied with the structures produced in the N_2 atmosphere. The laser pulse fluence and processing speed were kept constant and identical to those used for the production of the best performing structure, with total number of pulses delivered per spot being the only variable parameter. This resulted in some alterations of the surface geometry (see Fig. 8, Appendix A) accompanied by increase in the groove depth for larger number of pulses per spot. Figure 3(a) shows that a substantial increase in the spectral hemispherical emissivity response, compared to the untreated surface, can be achieved after as little as 140 pulses/spot, with the measured microcavity depth of ~ 160 μm, see Fig. 3(b). However further increase in the number of pulses to 1400, resulting in the microcavity depth of ~ 290 μm (Fig. 3(d)), does not yield any significant rise in the emissivity response, and is lower than the response achieved with the *in-air* processed surface. This can be attributed to the differences in the detailed microgeometry of the structures such as shape of microcones, microcavity apex angle and depth, Fig. 3(b) – 3(e). Earlier reports show that emissivity is highly sensitive to the detailed surface topography for surfaces with roughness exceeding the wavelength of light [32]. In this, so-called geometric region [32], geometrical optics principles are applied to analyze optical interactions and to predict emissivity response. It has been shown that periodical microgrooving not only increases specific surface area but also create favorable geometrical conditions for effective thermal dissipation, with V-shaped grooves performing better than rectangular or hemispherical microstructures by reducing the number of multiple radiation events between adjacent microchannels [33]. The apex angle of the groves also plays an important role in emissivity enhancement. A periodic V-shaped grooves with a 60° apex angle were shown to enhance normal emissivity by a factor of ~ 3.3. Further seven-fold increase in normal emissivity compared to a smooth surface was demonstrated with a groove angle of 30°, attributed to the increased surface roughness resulting in the increased number of radiation events for the identical measurement conditions, i.e. slit size [34]. On the other hand, presence of an oxide film on the surface affects its optical properties because of reduced interaction of the transmitted electromagnetic waves with electrons bounded to their nuclei in the dielectric oxide layer. Besides the compositional changes of the surface layer, oxidation generally leads to the increase of the surface roughness and interference effects that further enhance surface emissivity [14].

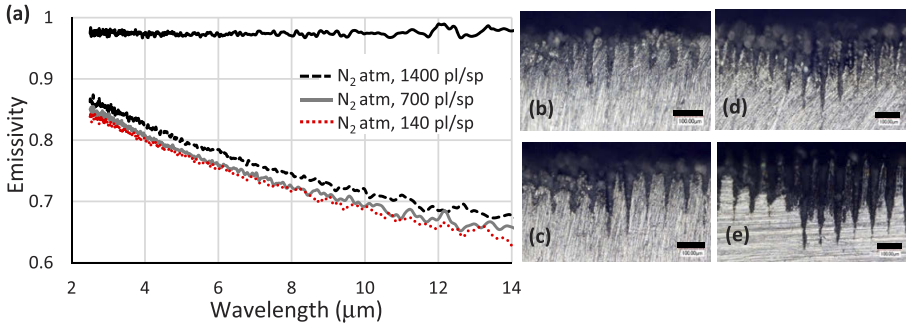

Fig. 3. (a) Room temperature spectral hemispherical emissivity of 304L steel surfaces processed with different number of pulses per spot (emissivity response of the best performing topography processed in the air atmosphere is shown in black). Surface cross sections after ns-laser structuring (*100-μm scale bar is shown in black*): (b) N_2 atmosphere, 140 pulses/spot, microcavity depth ~160 μm; (c) N_2 atmosphere, 700 pulses/spot, microcavity depth ~220 μm; (d) N_2 atmosphere, 1400 pulses/spot, microcavity depth ~290 μm); (e) air atmosphere, 1400 pulses/spot, measured microcavity depth ~350 μm.

To quantify the effects of surface treatment on the emissivity performance, total hemispherical emissivity in the spectral region from 2.5 to 14 μm ($\varepsilon_{2.5-14}$) was calculated from the spectral

Optical Materials EXPRESS

hemispherical emissivity data according to Eq. (2):

$$\varepsilon_{\lambda_1-\lambda_2}(T) = \frac{\int_{\lambda_1}^{\lambda_2} \varepsilon(\lambda, T) E_{b\lambda}(\lambda, T) d\lambda}{\int_{\lambda_1}^{\lambda_2} E_{b\lambda}(\lambda, T) d\lambda} \tag{2}$$

where $\varepsilon(\lambda, T)$ is the spectral hemispherical emissivity, $E_{b\lambda}(\lambda, T)$ is the Planck blackbody function.

The results summarized in Table 1 show that the observed emissivity increase is mostly due to the presence of the surface microstructure with less than 2% increase attributed to surface oxidation of AISI 304L stainless steel. Moreover, the laser-assisted microstructure engineering enables to achieve close to a blackbody performance, reaching a record high total emissivity value of 0.975 in the spectral region from 2.5 to 14 μm.

Table 1. Total hemispherical emissivity performance of 304L steel surfaces in the spectral region from 2.5 to 14 μm.

Surface Treatment	$\varepsilon_{2.5-14}$	Laser Structuring Parameters
Untreated	0.116	
Acid pickling	0.704	Air, 1400 pl/s
N_2 atmosphere	0.722	N_2, 1400 pl/s
320°C, 7-h oxidation	0.711	N_2, 1400 pl/s
320°C, 50-h oxidation	0.739	N_2, 1400 pl/s
320°C, 100-h oxidation	0.738	N_2, 1400 pl/s
600°C, 6-h oxidation	0.741	N_2, 1400 pl/s
1 repetition	0.693	N_2, 140 pl/s
5 repetitions	0.702	N_2, 700 pl/s
Air atmosphere	0.975	Air, 1400 pl/s

The effect of temperature on total emissivity of the best performing structure, shown in Fig. 4, was evaluated taking into account temperature-induced shifts of the Planck distribution only. The potential discrepancies between the total emissivity and its estimated value, calculated for the experimental data measured in a finite spectral region from 2.5 to 25 μm, were accounted for by calculating the lower and upper theoretical limits Eqs. (3) and (4).

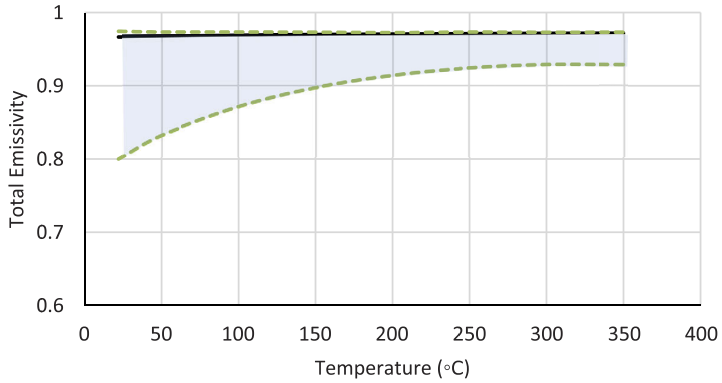

Fig. 4. Calculated temperature dependence of total hemispherical emissivity of 304L steel after laser structuring in *air* (laser fluence of ~3.6 J/cm^2, scanning speed of 10 mm/s, hatch distance 75 μm, and 1400 pulses/spot). Dashed curves are the upper and lower theoretical limits of total emissivity.

Optical Materials EXPRESS

The lower theoretical limit of total emissivity accounts for low spectral emissivity ($\varepsilon(\lambda, T) = 0$) in the unmeasured electromagnetic spectrum (i.e. from 0 to λ_1 and from λ_2 to ∞):

$$\varepsilon_l(T) = \frac{\int_{\lambda_1}^{\lambda_2} \varepsilon(\lambda, T) E_{b\lambda}(\lambda, T) d\lambda}{\int_0^{\infty} E_{b\lambda}(\lambda, T) d\lambda} = \frac{\int_{\lambda_1}^{\lambda_2} \varepsilon(\lambda, T) E_{b\lambda}(\lambda, T) d\lambda}{\sigma T^4} \tag{3}$$

where σ is the Stefan – Boltzmann constant, and T is the absolute temperature.

The upper theoretical limit accounts for the blackbody-like spectral emissivity ($\varepsilon(\lambda, T) = 0$) in the unmeasured electromagnetic spectrum:

$$\begin{aligned} \varepsilon_h(T) &= \frac{\int_0^{\lambda_1} E_{b\lambda}(\lambda, T) d\lambda + \int_{\lambda_1}^{\lambda_2} \varepsilon(\lambda, T) E_{b\lambda}(\lambda, T) d\lambda + \int_{\lambda_2}^{\infty} E_{b\lambda}(\lambda, T) d\lambda}{\int_0^{\infty} E_{b\lambda}(\lambda, T) d\lambda} = \\ &= f_1 + \frac{\int_{\lambda_1}^{\lambda_2} \varepsilon(\lambda, T) E_{b\lambda}(\lambda, T) d\lambda}{\sigma T^4} + f_2 \end{aligned} \tag{4}$$

where f_1 and f_2 are the blackbody radiation functions, representing the fraction of radiation emitted from blackbody in the wavelength region from 0 to λ_1 and from λ_2 to ∞ [2].

From Fig. 4, it can be seen that the total emissivity tends to increase with temperature. This accompanied by the decrease of the uncertainty range as the Planck distribution shifts towards shorter wavelengths.

To evaluate the microstructure stability, the *in-air* processed structure was subjected to thermal aging in air at 320°C for 96 hours. The spectral emissivity performance before and after the thermal aging remains almost identical in the spectral region from 2.5 to 14 μm, as shown in Fig. 5. The decrease of the spectral emissivity in the long-wavelength region can be attributed to minor changes in the surface nanotopography. Overall stability of the emissivity performance in the spectral region from 6 to 11 μm is attributed to the considerable size of microstructures making them less susceptible to surface diffusion at elevated temperatures.

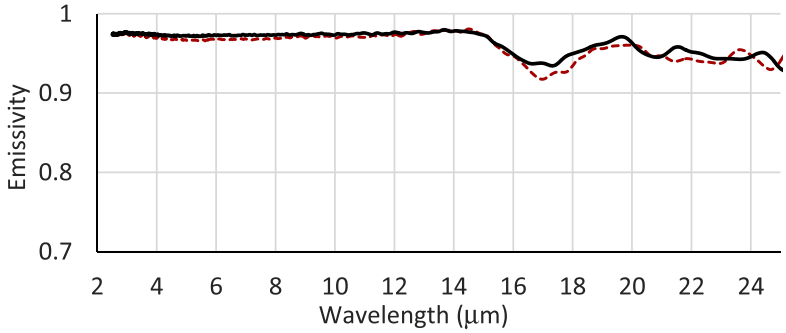

Fig. 5. Room temperature spectral hemispherical emissivity responses of the laser-structured 304L steel in *air* before (*solid black curve*) and after (*dotted red curve*) thermal aging in air at 320°C for 96 hours.

4. Conclusions

In summary, we demonstrated that ns-laser structuring is an effective method for control and manipulation of the spectral emissivity in a wide spectral region, which can be tailored to a wide range of metal surfaces. Total hemispherical emissivity of 0.97 was achieved on laser-structured 304L steel surfaces. It was found that surface topography has dominant effect on the emissivity performance. Stability of the emissivity performance after thermal aging at 320°C for 96 hours was verified.

Optical Materials EXPRESS

Appendix A. Supplementary material

This supplement provides details on the FT-IR spectroscopy, and the scanning electron microscopy of the laser structured surfaces.

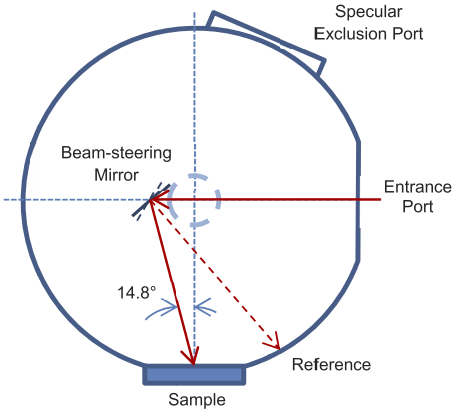

Fig. 6. Schematic of the emissivity measurements.

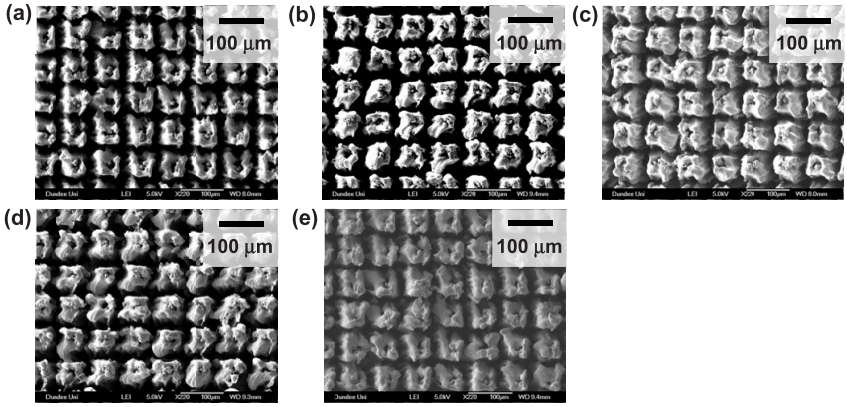

Fig. 7. Surface topographies of the laser-structured surfaces in N_2 before and after air oxidation: (a) before oxidation, (b) after 7-h oxidation at 320°C, (c) after 50-h oxidation at 320°C, (d) after 100-h oxidation at 320°C, (e) after 6-h oxidation at 600°C.

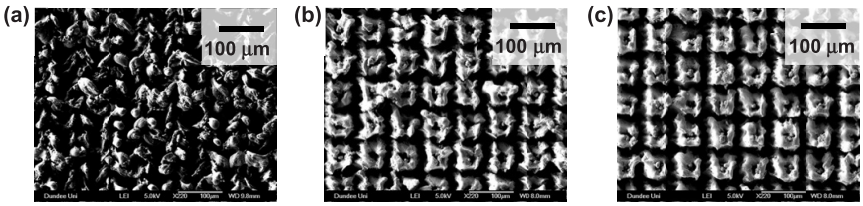

Fig. 8. Surface topographies of the laser-structured surfaces in N_2: (a) 140 pulses/spot, (b) 700 pulses/spot, (c) 1400 pulses/spot.

Optical Materials EXPRESS

Acknowledgements

Financial support for the emissivity measurement and SEM analysis at CERN was provided by the HL-LHC project.

Disclosures

The authors declare no conflicts of interest.

References

1. W. Li and S. Fan, "Nanophotonic control of thermal radiation for energy applications," Opt. Express **26**(12), 15995 (2018).
2. Y. S. Touloukian, Thermophysical Properties of Matter-The TPRC Data Series- 7 (1970).
3. J. Le Gall, M. Olivier, and J.-J. Greffet, "Experimental and theoretical study of reflection and coherent thermal emission by a SiC grating supporting a surface-phonon polariton," Phys. Rev. B **55**(15), 10105–10114 (1997).
4. J.-J. Greffet, R. Carminati, K. Joulain, J.-P. Mulet, S. Mainguy, and Y. Chen, "Coherent emission of light by thermal sources," Nature **416**(6876), 61–64 (2002).
5. H. Sai, Y. Kanamori, and H. Yugami, "High-temperature resistive surface grating for spectral control of thermal radiation," Appl. Phys. Lett. **82**(11), 1685–1687 (2003).
6. A. Narayanaswamy and G. Chen, "Thermal emission control with one-dimentional metallodielectric photonic crystals," Phys. Rev. B **70**(12), 125101 (2004).
7. I. Celanovic, N. Jovanovic, and J. Kassakian, "Two-dimentional tungsten photonics crystals as selective thermal emitters," Appl. Phys. Lett. **92**(19), 193101 (2008).
8. V. Rinnerbauer, A. Lenert, D. M. Bierman, Y. X. Yeng, W. R. Chan, R. D. Geil, J. J. Senkevich, J. D. Joannopoulos, E. N. Wang, and M. Soljačić, "Metallic photonic crystal absorber-emitter for efficient spectral control in high-temperature solar therophotovoltaics," Adv. Energy Mater. **4**(12), 1400334 (2014).
9. X. Liu, T. Tyler, T. Starr, A. F. Starr, N. M. Jokerst, and W. J. Padilla, "Taming the blackbody with infrared metamaterials as selective thermal emitters," Phys. Rev. Lett. **107**(4), 045901 (2011).
10. S.-Y. Lin, J. Moreno, and J. Fleming, "Three-dimentional photonic-crystal emitter for thermal photovoltaic power generation," Appl. Phys. Lett. **83**(2), 380–382 (2003).
11. T. Inoue, M. De Zoysa, T. Asano, and S. Noda, "Filter-free nondispersiveinfrared sensing using narrow-bandwidth mid-infrared thermal emitters," Appl. Phys. Express **7**(1), 012103 (2014).
12. E. Brodu, M. Balat-Pichelin, J. Sans, M. Freeman, and J. Kasper, "Efficiency and behavior of textured high emissivity metallic coatings at high temperature," Mater. Des. **83**, 85–94 (2015).
13. J. King, H. Jo, R. Tirawat, K. Blomstrand, and K. Sridharan, "Effects of surface roughness, oxidation, and temperature on the emissivity of reactor pressure vessel alloys," Nucl. Technol. **200**(1), 1–14 (2017).
14. H. Jo, J. L. King, K. Blomstrand, and K. Sridharan, "Spectral emissivity of oxidized and roughened metal surfaces," Int. J. Heat Mass Transfer **115**, 1065–1071 (2017).
15. B. Rousseau, M. Chabin, P. Echegut, A. Sin, F. Weiss, and P. Odier, "High emissivity of a rough Pr_2NiO_4 coating," Appl. Phys. Lett. **79**(22), 3633–3635 (2001).
16. J.-C. Panitz, M. Schubnell, W. Durisch, and F. Geiger, "Influence of ytterbium concentrationon the emissive properties of Yb:YAG and Yb:Y_2O_3," AIP Conf. Proc. **401**, 265–276 (1997).
17. L. M. Fraas, L. Ferguson, L. G. McCoy, and U. C. Pernisz, "SiC IR emitter design for thermophotovoltaic generators," AIP Conf. Proc. **358**, 488–494 (1996).
18. G. Apollinari, I. B. Alonso, O. Brüning, P. Fessia, M. Lamont, L. Rossi, and L. Tavian, *CERN Yellow Reports: Monographs* 4 (1) (2017).
19. M. Barnes, A. Adraktas, G. Bregliozzi, B. Goddard, L. Ducimetière, B. Salvant, J. Sestak, L. V. Cid, W. Weterings, and C. Y. Vallgren, "Operational experience of the upgraded LHC injection kicker magnets during Run 2 and future plans," J. Phys.: Conf. Ser. **874**, 012101 (2017).
20. L. Vega, A. Abánades, M. Barnes, V. Vlachodimitropoulos, and W. Weterings, "Thermal analysis of the LHC injection kicker magnets," J. Phys.: Conf. Ser. **874**, 012100 (2017).
21. A. Y. Vorobyev, V. Makin, and C. Guo, "Brighter light sources from black metal: significant increase in emission efficiency of incandescent light sources," Phys. Rev. Lett. **102**(23), 234301 (2009).
22. J. Yang, Y. Yang, B. Zhao, Y. Wang, and X. Zhu, "Femtosecond laser-induced surface structures to significantly improve the thermal emission of light from metals," Appl. Phys. B **106**(2), 349–355 (2012).
23. Y. Zhang, T. Fu, L. Fu, and C. Shi, "High temperature thermal radiation property measurements on large periodic micro-structured nickel surfaces fabricated using a femtosecond laser source," Appl. Surf. Sci. **450**, 200–208 (2018).
24. D. Starikov, C. Boney, R. Pillai, A. Bensaoula, G. Shafeev, and A. Simakin, "Spectral and surface analysis of heated micro-column arrays fabricated by laser-assisted surface modification," Infrared Phys. Technol. **45**(3), 159–167 (2004).
25. A. Abdolvand, R. W. Lloyd, M. J. Schmidt, D. J. Whitehead, Z. Liu, and L. Li, "Formation of highly organised, periodic microstructures on steel surfaces upon laser irradiation," Appl. Phys. A **95**(2), 447–452 (2009).

Optical Materials EXPRESS

26. G. Tang and A. Abdolvand, "Laser-assisted highly organised structuring of copper," Opt. Mater. Express **1**(8), 1425–1432 (2011).
27. *Cleaning and Descaling Stainless Steel, A Designers' Handbook Series 9001* (American Iron and Steel Institute, 1988).
28. N. Ohtsu, K. Kodama, K. Kitagawa, and K. Wagatsuma, "X-ray photoelectron spectroscopic study on surface reaction on titanium by laser irradiation in nitrogen atmosphere," Appl. Surf. Sci. **255**(16), 7351–7356 (2009).
29. P. Pou, J. Del Val, A. Riveiro, R. Comesaña, F. Arias-González, F. Lusquiños, M. Bountinguiza, F. Quintero, and J. Pou, "Laser texturing of stainless steel under different processing atmospheres: from superhydrophilic to superhydrophobic surfaces," Appl. Surf. Sci. **475**, 896–905 (2019).
30. F. Halden and W. Kingery, "Surface tension at elevated temperatures. II. Effect of C, N, O and S on liquid iron surface tension and interfacial energy with Al_2O_3," J. Phys. Chem. **59**(6), 557–559 (1955).
31. G. Cao, S. Weber, S. Martin, K. Sridharan, M. Anderson, and T. Allen, "Spectral emissivity of candite alloys for very high temperature reactors in high temperature air environment," J. Nucl. Mater. **441**(1-3), 667–673 (2013).
32. C.-D. Wen and I. Mudawar, "Modeling the effect of surface roughness on the emissivity of aluminum alloys," Int. J. Heat Mass Transfer **49**(23-24), 4279–4289 (2006).
33. J. Sun, J. Zhuang, H. Jiang, Y. Huang, X. Zheng, Y. Liu, and D. Wu, "Thermal dissipationperformance of metal-polymer composite heat exchanger with V-shape microgrooves: A numerical and experimental study," Appl. Therm. Eng. **121**, 492–500 (2017).
34. K. Kanayama, "Apparent directional emittances of V-groove and cicular groove rough surfaces," Heat Transfer – Jpn. Res. **1**, 1–22 (1972).